INTERNATIONAL ATOMIC ENERGY AGENCY
UNITED NATIONS EDUCATIONAL, SCIENTIFIC AND CULTURAL ORGANIZATION

INTERNATIONAL CENTRE FOR THEORETICAL PHYSICS
34100 TRIESTE (ITALY) - P.O.B. 586 - MIRAMARE - STRADA COSTIERA 11 - TELEPHONES: 224281 2 3 4 5 6
CABLE: CENTRATOM - TELEX 460392-1

SMR/93 - 39

AUTUMN COURSE ON GEOMAGNETISM, THE IONOSPHERE
AND MAGNETOSPHERE

(21 September - 12 November 1982)

EARTH-SPACE PREDICTION

K. DAVIES

Space Environment Laboratory
National Oceanic and Atmospheric
Administration
325 Broadway
Boulder, Colorado 80303
U.S.A.

These are preliminary lecture notes, intended only for distribution to participants. Reprints or extra copies are available from Room 230.

International Centre for Theoretical Physics

Autumn Course on Geomagnetism, the Ionosphere and Magnetosphere

Workshop on Radio Propagation in the Tropics

Lecture V

Earth-Space Propagation

by

Kenneth Davies

5.1 Introduction

The launch of Sputnik I in 1957 opened up an entirely new era in telecommunications -- satellite transmission systems. It was quickly realized that satellites, because of their wide coverage of the earth, held great potential for radio communications. This is especially so for satellites in a synchronous orbit: one in which the satellite rotates with the earth at an altitude of $\approx$ 35000 km. Such satellites are now used regularly for telephone and television communications. For further information on ionospheric studies using satellite beacons see the reviews by Evans (1977) and Davies (1980).

One big advantage of satellite systems, or so it was thought, is that sufficiently high frequencies could be used so that the radio signals would not be disturbed by the ionosphere. In the early days of satellite telemetry, frequencies in the VHF band were selected ($\approx$ 137 MHz). Almost immediately the users found that the signals fluctuated because of diffraction by ionospheric irregularities. This phenomenon was called scintillation since it had already been observed on radio signals traversing the ionosphere from galactic sources. Also noted was polarization fading of the electric fields of the radio signals (Faraday rotation).

Thus the notion that satellite systems could be immune to ionospheric effects was shaken and in the 1960's decisions were made to go to still higher frequencies (to 4 and 6 GHz) to finally get away from the troublesome ionosphere.

However, it was soon found that, while these frequencies provided a considerable reduction of adverse ionospheric effects, scintillations could still be troublesome in equatorial regions on some evenings around the equinoxes.

The electrons in the ionosphere reduce the group speed of the radio signals and, therfore, can be a major limiting factor in the range accuracy of modern satellite navigation systems. On frequencies of about 100 MHz and higher the major effect of the ionosphere on transionospheric propagation are: (1) time delays over and above the free space values; (2) polarization rotation of linearly polarized waves; (3) angular refraction or bending of the ray path from a straight line; -- see Figure 5.1-- (4) phase advance of the carrier with respect to the free space value.

5.2 Total Electron Content

Figure 5.2 illustrates some of the salient propagation effects of transionospheric radio, namely: Faraday rotation and scintillation. The rotation of the electric vector results from the different characteristics of the ordinary and extraordinary waves. In Lecture #1 we saw that when a radio wave enters the ionosphere it is split up into two characteristic waves (O and X) that can propagate as independent waves. These waves have different refractive indices and hence, different wavelengths, different phase velocities and opposite senses of rotation. In free space a linearly polarized wave can be split into two oppositely rotating circularly polarized waves which travel with the same speed and, therefore, there is no net change in the direction of the resultant electric field. When a VHF wave is emitted from a satellite, ($f \gg f_H$, $f \gg f_N$) equation 1.26 shows that $R_{\mp} = \mp i$ which shows that the polarizations are circular. Hence the power is equally divided between the O and X waves. As these waves propagate through the ionosphere we get the picture, depicted in Figure 5.3, in which the component waves, traveling a distance s, produce a net rotation Ω of the electric field where

$$\Omega = \frac{1}{2}(\Omega_+ - \Omega_-)$$

$$= \frac{\pi s}{\lambda_0}(\mu_+ - \mu_-) \qquad 5.1$$

where $\lambda_0 = \frac{c}{f}$ is the free space wavelength μ_+, μ_- are the refractive indices of the O and X waves. Equation (1.16) gives (see Davies, 1969, Chapter 9).

$$\mu_+^2 - \mu_-^2 = \frac{X\sqrt{Y_T^4 + 4(1-X)^2 Y_L^2}}{(1-X)(1-Y_L^2) - Y_T^2} \qquad 5.2$$

Since $X \ll 1$ and $Y_{L,T} \ll 1$

$$\mu_+ - \mu_- \approx \frac{XY_L}{1-Y_L^2} \approx XY_L \qquad 5.3$$

and

$$\Omega \approx \frac{\pi s}{c}\frac{f_N^2 f_L}{f^2} = \frac{2.365\times10^4}{f^2} NB_0 \cos\theta s \qquad 5.4$$

where N is the electron density (assumed constant along s) B_0 is the strength and θ the direction of the earth's magnetic field.

The quantity Ns is the total number of electrons in a cylinder of 1 m^2 cross section and length s. It is known as the total columnar electron content or simply the total electron content (TEC). The Faraday rotation is proportional to:

(a) the total content along the path

(b) the magnetic field strength

(c) inverse frequency squared.

It is important to notice that equation 5.4 is not applicable when the propagation is perpendicular to $\underline{B}_0$, i.e. $\theta \approx 90°$.

To an observer looking along the magnetic field component in the direction of wave propagation the resultant E vector traces out on helix with a right-handed sense of rotation -- the thumb being in the direction of the magnetic field. Hence, to a fixed observer looking up the magnetic field in the northern hemisphere an increase in electron content will produce a counterclockwise rotation of the electric vector as illustrated in Figure 5.4.

Equation 5.4 can be put into a form which enables the electron content to be determined from measurements of the Faraday rotation viz

$$\Omega = 2.365 \times 10^4 f^{-2} \bar{M} N_F \qquad 5.5$$

where $\bar{M} = \overline{B_0 \cos\theta \sec\chi}$ is an average value of the longitudinal component of the magnetic field along the ray path. Titheridge (1972) has shown that, for all practical purposes, $\bar{M}$ can be taken as the value of $B_0 \cos\theta \sec\chi$ at 420 km. N_F is called the Faraday content.

Typical values of polarization rotation for a middle latitude station and a geostationary satellite are shown in Figure 5.5. This is applicable down to magnetic latitudes of the order of 10°. Decreases in the M factor brought about by the decrease of B_0 in low latitudes, and the larger θ, are compensated by the larger TEC.

For satellite navigation and communication designers the Faraday rotation is a nuisance. A linearly polarized signal from a satellite may suffer just the right amount of Faraday rotation that it arrives perpendicular to a linear receiving antenna producing no signal at the antenna terminals. This problem can be overcome by using circular polarization.

5.3 Time Delay

When the magnetic field and collision effects are negligible the group refractive index -- see equation (1.10) -- is given by $1/\mu$ and the group propagation

time is given by equation (1.12)

$$\text{or} \qquad T_g = \frac{1}{c} \int \mu^{-1} ds \qquad 5.6$$

since $\alpha \overset{\sim}{=} 0$. Substitution of equation (1.17) gives the following time delay, ΔT, over the free-space value of the transit time.

$$\Delta T = (40.3/cf^2) \times (\text{TEC}) \text{ sec} \qquad 5.7$$

where c is in meters/sec, f in Hertz and the TEC is in electrons per meter squared. Extreme value of this content vary from 10^{16} el/m^2 to 10^{19} el/m^2. A plot of excess time delay versus frequency is shown in Figure 5.6. We see that, on a frequency of 1 GHz a TEC of 10^{18} el/m^2 (a value frequently exceeded in low and middle latitudes), a time error of 134 nanoseconds or 40.2 meters will be encountered by a navigation system. On 100 MHz this same TEC value will produce an error of about 4 km. Thus, the TEC is of importance in precision satellite navigation.

The total electron content can be estimated from numerical maps of the F2 critical frequency (since $N_m = 1.24 \times 10^{10} \text{foF2}$), together with a layer shape, which give a global representation of the diurnal, seasonal, and solar cycle variations. Thus systems design engineers are able to determine the potential effects of the ionosphere on any new satellite navigation system. A layer shape parameter may be the slab thickness τ defined by

$$\text{TEC} = \tau \times N_m \qquad 5.8$$

which is the thickness of a slab of plasma of constant density N_m that gives the observed TEC. A typical slab thickness in low latitudes would be 500 km.

As in the case of other ionospheric parameters (e.g. foF2, fE_s) the TEC is highly variable from day to day as seen in Figure 5.7. Some, but no means all, of the day-to-day variability is caused by magnetic storms. To a first approximation, the departures of hourly TEC values from the monthly median is Gaussian (Klobuchar 1978 AGARD). A good working value for systems engineers to use for design purposes for the standard deviation of ionospheric time delay is 25 per cent.

Individual days may have values far in excess of the standard deviation as, for example, during storms when the TEC may be either greatly enhanced, on day one, and greatly depressed on succeeding days. For these extreme cases, statistics are unreliable. Any system design engineer must be careful to consider worst case TEC values, even though they occur infrequently.

If a navigation system has two frequencies f_1 and f_2, equation (5.7) suggests a method by which the excess ionospheric time delay can be measured, and automatically taken care of, without the user's participation. Let $f_1 > f_2$, let δT_1 and δT_2 refer to the delays on f_1 and f_2 respectively then

$$(\delta T_2 - \delta T_1) = \delta T_1 (f_1^2 - f_2^2)/f_2^2 \qquad 5.9$$

where we assume that f_1 is the normal operating frequency. $(\delta T_2 - \delta T_2)$ is obtained from the differences of the simultaneous measurements of the range on f_1 and f_2. The quantity $f_2^2/(f_1^2 - f_2^2)$ is called the ionospheric scaling factor. For practical purposes it is desirable to have f_1/f_2 as large as possible. Typical values of f_1 and f_2 may be 1.6 GHz and 1.2 GHz or 400 Hz and 350 MHz.

The ionosphere affects the carrier phase of radio waves passing through it. Actually the radio phase is advanced (because $\mu < 1$) with respect to the free space value. This relative phase advance is given by

$$\phi = \frac{1.34 \times 10^{-7}}{f} \text{ (TEC) cycles.} \qquad 5.10$$

where f is in Hertz. The relative phase advances $\Delta\phi$ on two signals of frequencies f_1 and f_2 is:

$$\Delta\phi = \phi_2 \quad \phi_2 = \frac{1.34 \times 10^{-7}}{f_1} (m - 1)(TEC) \qquad 5.11$$

where $m = f_1/f_2$.

Take $f_1 = 2f_2 = 400$ MHz, TEC = 10^{17} m^{-2}

$$\Delta\phi \approx 33 \text{ cycles.}$$

This illustrates one of the major problems in the measurement of radio phase namely the resolution of the number of cycles -- the cycle ambiguity.

Time variations of radio phase produce doppler shifts Δf where

$$\Delta f = \frac{d\phi}{dt} = \frac{1.34 \times 10^{-7}}{f} \frac{d(TEC)}{dt} \qquad 5.12$$

The doppler shift contains a small part due to the rate of change of TEC as the path changes and a large part due to the relative motion of the satellite and the receiver. The former is given by equation (5.12). For all practical considerations Δf is small (e.g. 0.1 Hz on a carrier frequency of 1.6 GHz, 0.3 Hz on 400 MHz).

5.4 Models of TEC

Instead of direct measurement of time delay by the two frequency method, the design engineer may prefer to use a model of TEC to estimate the time delay to be allowed for. Since models usually represent average conditions, updated values (e.g. critical frequencies from ionograms) of some model parameters can yield improvement. Empirical models are available such as the numerical maps (ITS-78 Jones and Stewart 1970) giving foF2 (and, hence, N_m). The slab thickness parameter can be obtained from models of the electron density distribution with height such as the Bent et.al. (1975) model in which topside thickness was obtained from Alouette ionograms. This model, unfortunately, depends heavily on data near the 70°W meridian but currently it is the best model. Klobuchar (1975) has produced an algorithm of time delay for users which is designed to correct for 50% of the effects. His model fits the monthly average TEC at times of day when the delays are greatest. No attempt is made to correct for day-to-day fluctuations.

In the equatorial regions, there are few data which go into the models. These regions are very important for world-wide navigation systems that required correction for ionospheric effects because the highest TEC values occur there.

The existing models of TEC represent, fairly well, the monthly averages at some locations, any significant improvement upon their average climatology may come from near-real time updating. Dulòng (1977) has shown that useful improvements can be made with data 3 hours old only at high sunspot numbers.

5.5 TEC near the Magnetic Equator

Faraday measurements at the magnetic equator are difficult to interpret in terms of Faraday electron content because the propagation is nearly transverse to the magnetic field where the concept of Faraday rotation loses its usual meaning (Davies 1969, Section 9.4.3).

Measurements of total electron content, from time delay measurements, were made at Ootacamund in South India using the ATS6 radio beacon in 1975 and 1976. Some examples of the diurnal variation of N_T are shown in Figure 5.8. At sunspot minimum, N_T rises very rapidly, from a deep presunrise low, through mid-morning (1000 LT) to a maximum usually in the afternoon followed by a decay and a secondary maximum in the late afternoon. The mid-day maximum is of the order of 3×10^{17} el/m^2 when allowance is made for obliquity of the path. Donnelly, Davies and Anderson (1979) show that the TEC variations at Ooty were essentially similar to those of the profiles at Jicamarca obtained by the incoherent scatter radar, see Figures 2.15 and 2.16.

5.6 Plasmaspheric Content

The total electron content measured by time delay (or phase) in general differs from the Faraday content. The former is the true total content N_T while the latter is weighted by the magnitude and direction of the magnetic field.

In the case of a geostationary satellite (near the magnetic equator) and an observer at a latitude greater than about 10° the Faraday content N_F represents the electron content up to an altitude of about 2000 km. The difference between these contents gives the plasmaspheric, or protonospheric, content N_p

$$\text{i.e.} \quad N_p = N_T - N_F \qquad 5.13$$

This technique has been used in conjunction with the ATS6 radio beacon (Davies 1980). Some models of the electron density distribution obtained by this method are shown in Figure 5.9. The plasmasphere, or protonosphere, consists essentially of electrons and thermal protons. In middle latitudes, it acts as a reservoir for the F2 layer. During the day, when ions are produced in the ionosphere, plasma diffuses upward into the plasmasphere where the loss rate is very low. At night the electron content of the ionosphere falls but downward settling of plasma from above prevents complete disappearence of the F layer. Because plasma cannot diffuse across a magnetic field this mechanism is inoperative right at the magnetic equator and this has been advanced as a reason that foF2 there falls to very low values just before dawn (see Figure 2.16).

The diurnal variation of N_p varies geographically. Over the USA it tends to peak during the night, at least at sunspot minimum, whereas in Europe it peaks in the day (Davies 1980). The ratio N_p/N_T varies from about 0.1 during the day to about 40% at night mostly caused by the variation of N_T. Thus a rough relationship between N_T at any local time LT and N_F is given by

$$N_T(LT) = a\, N_F(max) + N_F(LT) \qquad 5.14$$

where N_F (max) is the monthly mean diurnal maximum of N_F.

Unfortunately measurements of N_p near the magnetic equator are unreliable because propagation is nearly transverse to the magnetic field and, therefore, the Faraday content is not well defined.

The plasmaspheric content is sensitive to magnetic storms. Kersley et. al. (1978b) has shown that, on the average, N_p reaches a minimum on day 3 of the storm and recovers slowly over one to two weeks, see Figure 5.10.

5.7 Scintillation

5.7.1 Introduction

A radio signal traversing the ionosphere will be modified by irregularities with sizes from a few (3) meters to a few kilometers. Scintillations are variations of amplitude, phase, polarization and angle of arrival. Scintillations can be severe and present problems to the radio operator. Transionospheric effects of scintillation have been observed on frequencies from 20 MHz through 6 GHz. Scintillations are particularly severe in tropical regions during evenings around the equinoxes and in the auroral zones.

5.7.2 Amplitude scintillations

Amplitude scintillations can be characterized by a depth of fading and a fading period or frequency. A widely used index, S_4, is the root mean square of the power, P, divided by the average power $\bar{P}$ (Briggs and Parkin, 1963).

$$S_4 = \sqrt{\frac{\overline{(P - \bar{P})^2}}{\bar{P}}} \qquad 5.15$$

For simplicity of scaling a scintillation index, SI, has been defined

$$SI = \frac{P_{max} - P_{min}}{P_{max} + P_{min}} \qquad 5.16$$

(Whitney el. al. 1969). An example of amplitude fading is shown in Figure 5.9.

A global picture of scintillation is shown in Figure 5.11 which shows the important equatorial and auroral/polar regions. The equatorial scintillations are, on the whole, stronger than those in high latitudes. Scintillations occur in middle latitudes but they are less intense than elsewhere and do not present a serious problem. Scintillations, at night, are predominantly an

F-layer phenomenon with irregularities covering the range 200 km to 600 km in high latitudes. However, daytime scintillation in low latitudes can also be produced by sporadic E (Rastogi et. al. 1977). In high latitudes scintillation increases strongly with magnetic disturbance (storms). The F region irregularity zone reaches its lowest latitude of 57° before midnight. The highest scintillation indices ($S_4 \gtrsim 1.0$) occurred during storms, including some in daytime (Aarons, 1978). The mean scintillation index depends on geomagnetic location. At latitudes above 53°, a higher K_p is associated with higher scintillation while below 53° there is a small decrease of S_4 with increase of K_p.

5.7.3 Equatorial scintillations

In the equatorial region, the typical development of scintillation is often abrupt -- see Figure 5.12 -- sometimes occurring within a single fade. Fading of the order of 20 dB below the mean is observed. Rapid and deep fading characterizes the beginning of the activity. As the night progresses, the scintillation may become more sporadic with intervals of shallow fading. The small scale irregularities are contained in large scale patches that move across the raypath. Toward the end of the scintillation activity, the scintillations change character in which long fades may stay below fade margins of 6 dB for 5 to 10 seconds.

Scintillation patterns vary greatly, one pattern shows a patchy nature in which scintillation starts and stops several times in one night, with the patch moving through the raypath in times of the order of 20 mins. to several hours. Similar lifetimes of scintillations have been noted in HF transequatorial studies by Crochet (1972) and Röttger (1973). In the equatorial region, there are large scale irregularity patches (several hundreds of km E W and many times that N S) which contain small scale irregularities, some as small as 3m to 1m, which produce VHF and microwave scintillation.

During evening hours, when scintillation is most intense, incoherent scatter radar observations at Jicamarca, Peru show the existence of plumes in the topside of the ionosphere, Figure 5.13. The time history of the plume shows an eastward drift of an irregularity zone. These plumes have been seen up to heights of the order of 800 km which is the limit of the radar. A sample time history is as follows (Aarons 1978). The scintillation starts shortly after sunset with UHF scintillations of 5dB peak-to-peak values typical and fading rates around 10/min. During the build-up of the plumes the scintillation depth increases to around 20 dB peak-to-peak with fading rates greater than 10/min. It is during this stage that microwave scintillations are observed. After formation, an irregularity structure moves east at speeds between 50 and 150 m sec^{-1}. During this phase the scintillation depth decreases. Observations suggest that the eastward motion diminishes near midnight. The plume forms a patch of irregularities that extend along the magnetic field like a banana -- Figure 5.14 -- with an east-west size greater than about 100 km, vertical height of 50 to several hundred km and north-south dimension of the order of 2000 km.

In situ (satellite) measurements of ion density in the F region (225 km) show severe depletions. Patches show both depletions and scintillations on Faraday rotation. Some depletions are more than 90 per cent (Aarons 1982). Scintillation data show equinoctial maxima. In general, increased magnetic activity inhibits scintillation before midnight (May-June) for the region (0°-70° W) and November-January (135-180°E). After midnight the scintillation activity, in general, increases slightly during magnetic storms. On the other hand Deshpande et. al. (1976) report that during the storm of January 10-11, 1976 severe scintillation of ATS6 signals were observed al all but the most northern stations in India. Scintillations on 136 MHz, 1.7 GHz, 4 GHz and even on 11.5 GHz were observed in Japan during the storm of February 15, 1978 by Ogawa et. al. (1978).

Recent observations during solar maximum (1979-81) show that scintillation maximizes at the peaks of the equaorial anomaly rather than at the geomagnetic dquator. Scintillations of up to 9 dB have been observed on the 4 GHz COMSAT downlink passing through an anomaly crest.

5.8 Ringing Irregularities

On some occasions a type of fading is observed (in both middle and low latitudes) that is characterized by a central minimum and amplitude fluctuations on one or both sides of the minimum, see Figure 5.15. These may be isolated or in tandem and they have been successfully modeled by using small scale ($\tilde{\sim}$ 200-500 meter) cylindrical lenses (Davies and Whitehead 1977, Heron 1979, Trivedi et. al. 1978). An important feature of this type of lens is that although the lens itself may be a few hundred meters across the diffraction pattern on the ground may be tens of km wide.

5.9 Near Real-time Maps

Observations (e.g. Faraday rotation) using a combination of geostationary and polar orbiting satellites can be used to construct maps of the TEC over continental size regions. An example of such a map, developed by Davies et. al. (1977) is shown in Figure 5.16. The geostationary satellite enables the measurement of TEC as a function of time at fixed latitudes whereas the polar orbiting satellites give latitudinal coverage at essentially fixed longitudes. These contour maps show the presence of large scale features such as troughs, ridges, holes in the TEC structure and how they vary from day to day. Somewhat similar maps have been constructed over India (Klobuchar et. al. 1977, Singh et. al. 1978).

References

Aarons, J., 1978, Ionospheric Scintillations: an introduction, AGARD Lecture Series, LS-93, Lecture 8.

Aarons, J., 1982, Global morphology of Ionospheric scintillations, Proc. of ISEE, April 1982, Vol. 17, pp. 360-378.

Bent, R. B., S. K. Llewellyn, G. Nesterizuk, and P. E. Schmid, 1975, The development of a highly successful worldwide empirical ionospheric model and its use in certain aspects of space communications and worldwide total electron content investigations, in Effects of the Ionosphere on Space Systems and Communications, editor J. M. Goodman, Naval Research Laboratory, U. S. Gov't Printing Office No. 008-051-00064-0.

Briggs, B. H. and I. A. Parkin, 1963, On the variation of radio star and satellite scintillations with zenith angle, J. Atmos. Terr. Phys., 25, (6), 339-365.

Crochet, M., 1972, Propagation transequatoriale en dehors due grand cercle en ordes decametriques, Partie 1: Mise en evidence at morphologie, Ann. Geophys., 28, 27-35.

Davies, K., 1969, Ionospheric Radio Waves, Blaisdale Publishing Co.

Davies, K., 1980, Recent progress in satellite radio beacon studies with particular emphasis on the ATS-6 radio beacon experiment, Space Sci. Rev., 25, 357-430.

Davies, K., G. K. Hartman and R. Leitinger, 1977, A comparison of several methods of estimating the columnar electron content of the plasmasphere, J. Atmos. Terr. Phys., 39, 571-580.

Davies, K. and J. D. Whitehead, 1977, A radio lens in the ionosphere, Jour. Atmos. Terr. Phys., 39, 383-387.

Deshpande, M. R., R. G. Rastogi, M. Singh, H. S. Gurm, A. V. Jouve, R. K. Rai, A. R. Join, B. N. Bhargava, V. M. Patwari and B. S. Subbaras, 1976, Some new phenomena observed during magnetic storms and solar flares at low and equatorial latitudes using ATS6 radio beacon investigations, in The Geophysical Uses of Satellite Beacon Observations, 412-415, editor, M. Mendillo, Boston University.

Donnelly, R. F., K. Davies and D. N. Anderson, 1979, The equatorial total electron content and shape factor, J. Geophys. Res., 84, 7359-7364.

Dulong, D. D., 1977, Reduction of the uncertainty of radar range correction, AFGL-TR-77-0125.

Evans, J. V., 1977, Satellite beacon contributions to studies of the structure of the ionosphere, Rev. Geophys. Space Phys., 15, 325-350.

Heron, M. L., 1979, Diffraction from discrete and homogeneously structured ionospheric irregularities, Radio Sci., 14, (1), 97-102.

Jones, W. B., and F. G. Stewart, 1970, A numerical model for global mapping of plasma frequency, Radio Sci., 5. 773-784.

Kersley, L., H. Hajeb-Hosseiniel, and J. K. Edwards, 1978b, Post-geomagnetic storm protonospheric replenishment, Nature, 271, 429-430.

Klobuchar, J. A., 1975, A first-order, worldwide, ionospheric time-delay algorithm, AFCRL-TR-75-0502.

Klobuchar, J. A., K. N. Iyer, H. O. Vats and R. G. Rastogi, 1977, A numerical model of equatorial and low latitude total electron content for use by satellite tracking systems for ionospheric corrections, Indian J. Radio Space Phys., 6, 159-164.

Klobuchar, J. A., 1978, Ionospheric effects on satellite navigation and air traffic control systems, AGARD Lecture Series LS-93, Lecture 7.

Ogawa, T., M. Fujita, J. Awaka and K. Sinno, 1978, Severe disturbances of VHF and GHz waves from geostationary satellites during a magnetic storm.

Rottger, J., 1973, Wave-like structures of large scale equatorial spread-F irregularities, J. Atmos. Terr. Phys. 35, 1195-1206.

Singh, M., H. S. Gurm, M. R. Deshpane, R. G. Rastogi, G. Sethia, A. J. Jain, A. V. Janve, A. K. Rai, V. M. Patwari and B. S. Subbarao, 1978, Total Electron content at low latitudes, Proc. Indian Acad. Sci. 87A, (3), 47-55

Titheridge, J. E., 1972, Determination of ionospheric electron content from the Faraday rotation of geostationary satellite signals, Planet. Space Sci., 20, 353-369

Trivedi, A. I., M. R. Deshpande and H. O. Vats, 1978, Diffraction of ATS6 signals by isolated ionospheric irregularities -- some new aspects, Proc. Indian Acad. Sci. 87A, (7), 165-172

Whitney, H. E., C. Malik and J. Aarons, 1969, A proposed index for measuring ionospheric scintillations, Planet. Space Sci., 17, 1069-1073.

Figure Captions

Figure 5.1 Ray path refraction in transionospheric propagation.

Figure 5.2 Ionospheric effects on transionospheric radio propagation.

Figure 5.3 Faraday rotation as the superposition of oppositely rotating circularly-polarized waves.

Figure 5.4 Faraday rotation of ATS-6 signals, seen from Boulder.

Figure 5.5 Approximate Faraday rotation as a function of frequency for a northern middle latitude station with the ray path in a magnetic meridian.

Figure 5.6 Ionospheric time delay versus frequency for several TECs.

Figure 5.7 Daily curves of N_F, N_T and N_p and monthly median values, ATS6-Graz, Austria.

Figure 5.8 Diurnal variations of TEC at Ootacamund, India.

Figure 5.9 Electron density profiles obtained from satellite beacon measurements, Boulder.

Figure 5.10 Storm behavior of the plasmasphere contents.

Figure 5.11 Morphology of scintillation fading.

Figure 5.12 Abrupt changes in scintillation.

Figure 5.13 Incoherent scatter plumes and satellite radio scintillation near the equator.

Figure 5.14 Three-dimensional patch model of equatorial ionospheric irregularities.

Figure 5.15 Fading of ATS6-Boulder signals caused by an intense irregularity.

Figure 5.16 Contour map of TEC in latitude versus time, in TEC units of 10^{15} m^{-2}. Separation of solid lines $\approx$ 20 x 10^{15} m^{-2}.

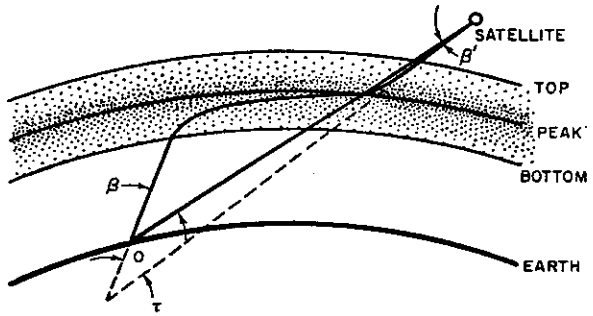

Fig. 5.1 Ray path refraction in transionic propagation

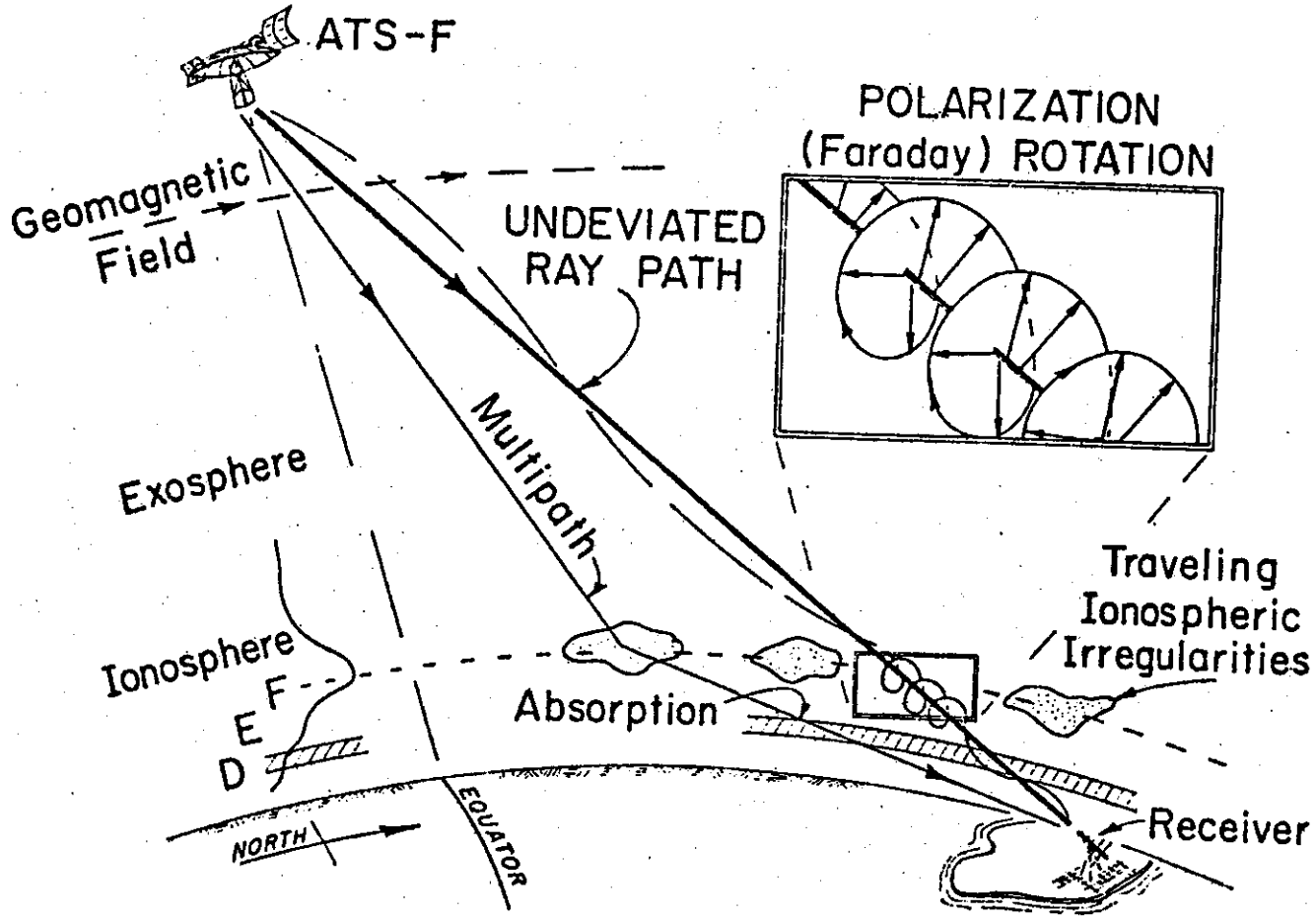

Fig. 5.2 Ionospheric effects on transionospheric radio propagation.

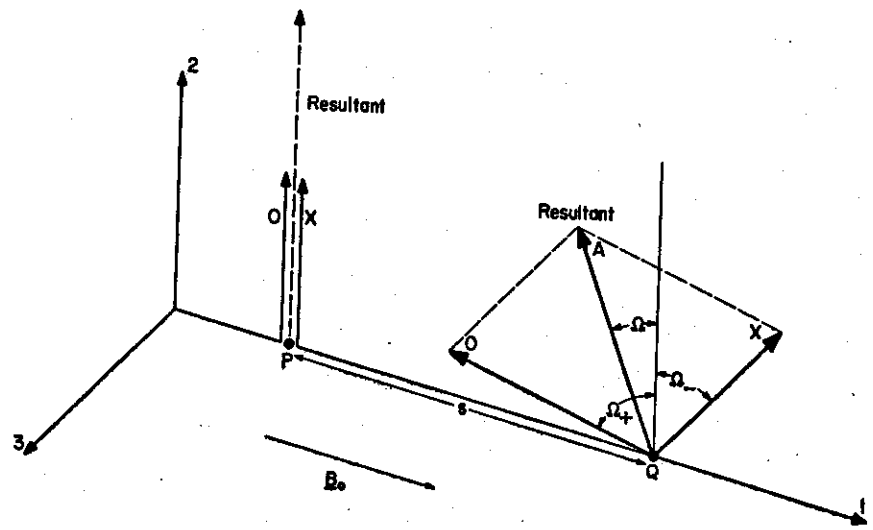

Fig. 5.3 Faraday rotation as the superposition of oppositely rotating circularly-polarized waves.

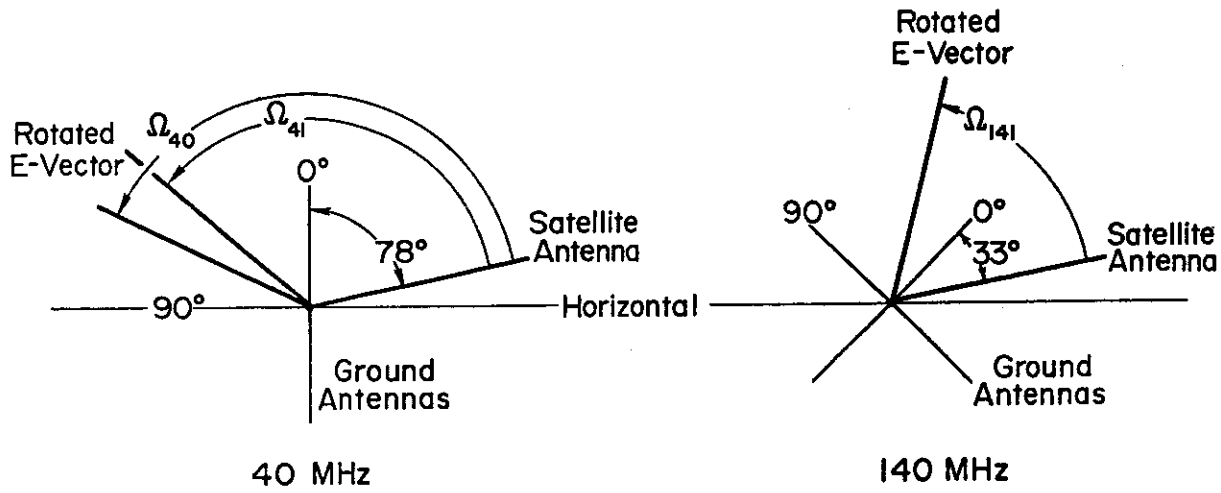

Faraday Rotation, as seen from Boulder, is counterclockwise.

Fig. 5.4 Faraday rotation of ATS-6 signals, seen from Boulder.

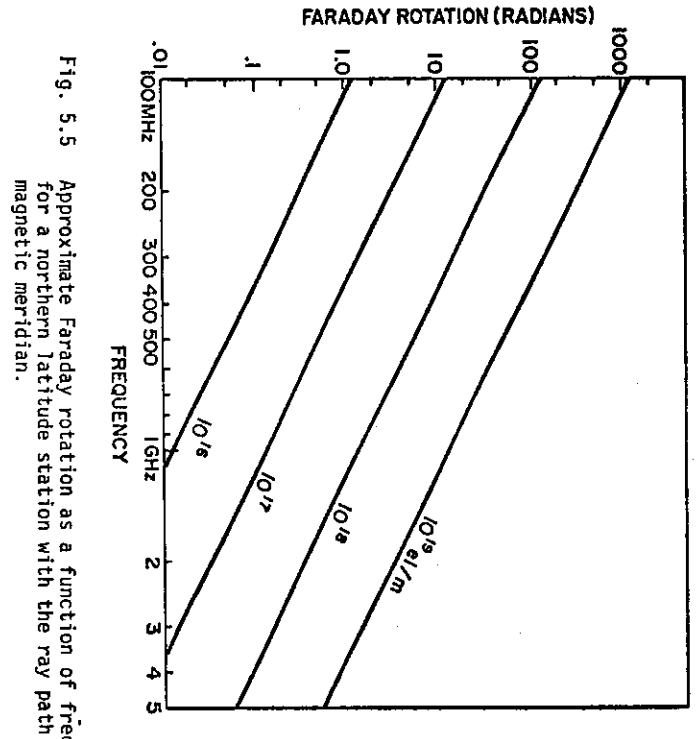

Fig. 5.5 Approximate Faraday rotation as a function of frequency for a northern latitude station with the ray path in a magnetic meridian.

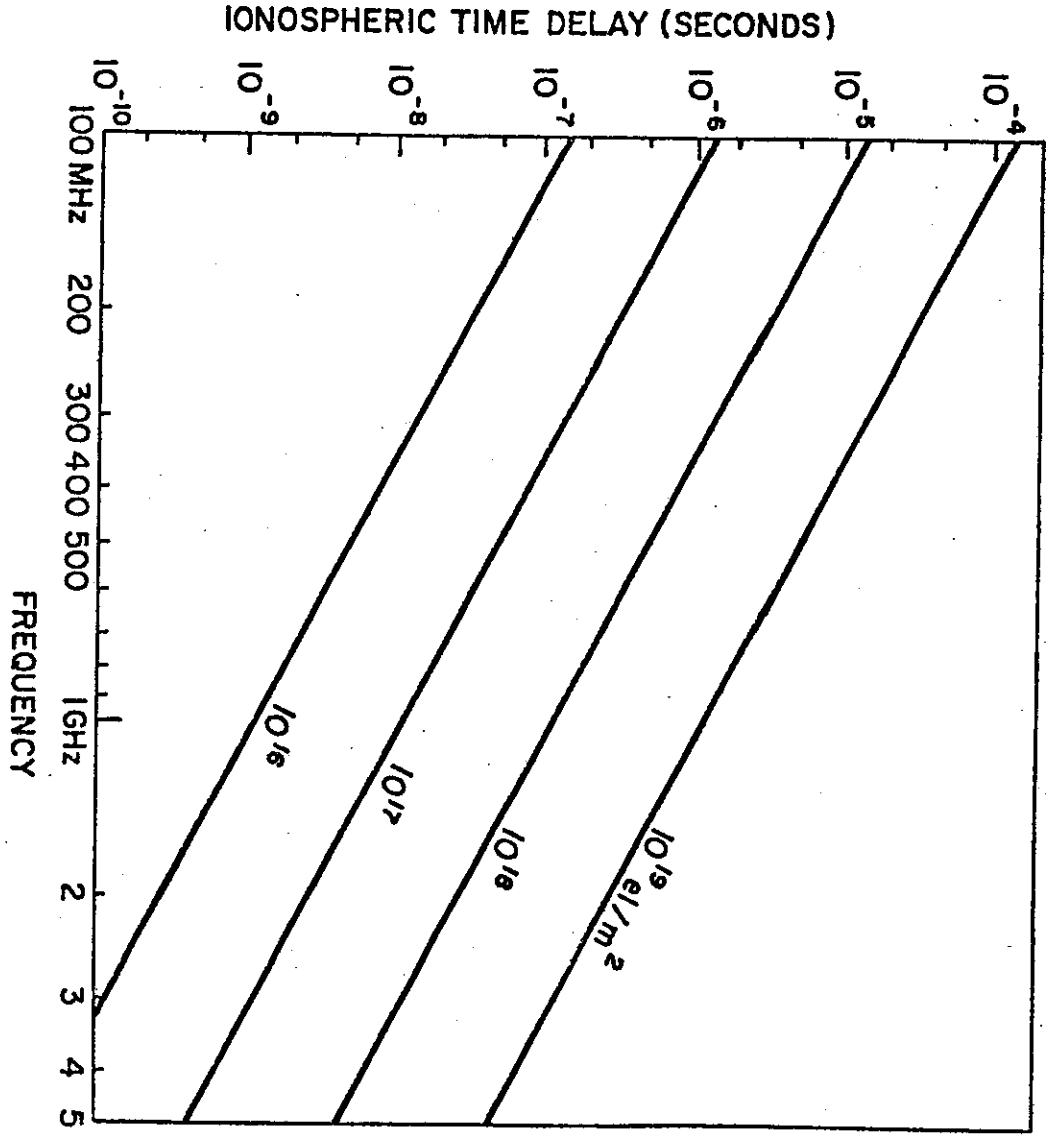

Fig. 5.6 Ionospheric time delay versus frequency for several TECs.

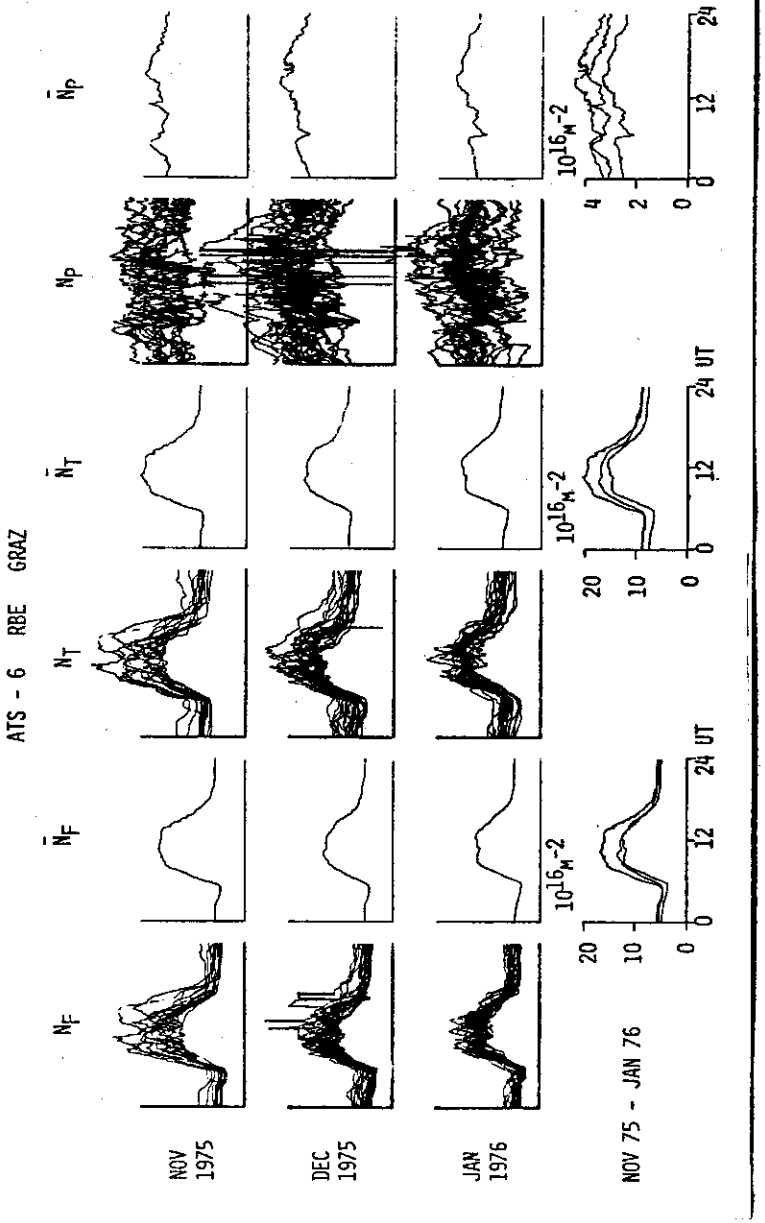

Fig. 5.7 Daily curves of N_F, N_T and N_p and monthly median values, ATS6-Graz, Austria.

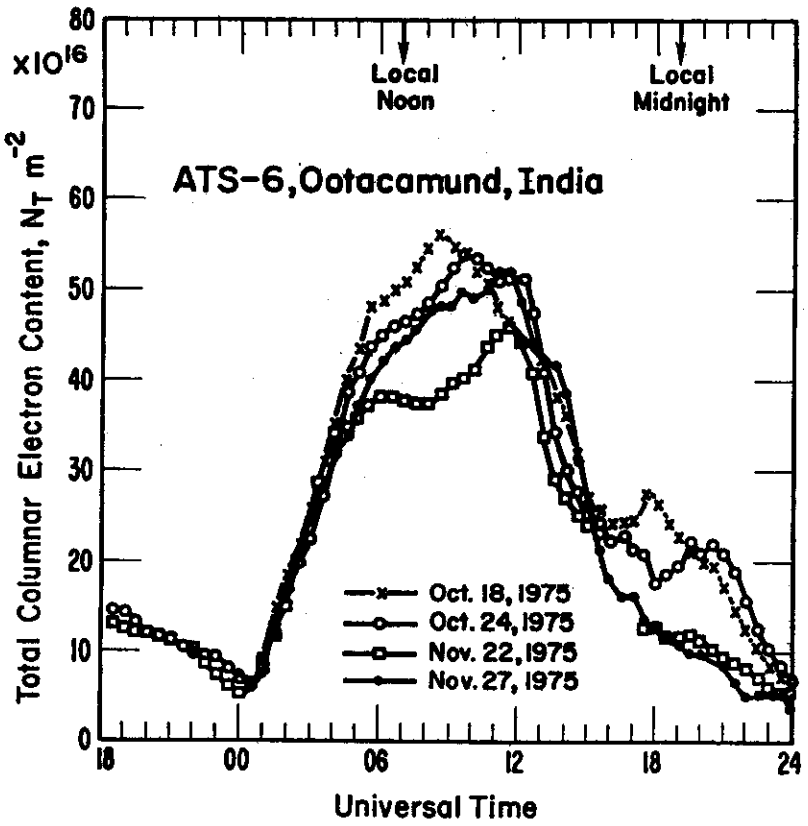

Fig. 5.8 Diurnal variations of TEC at Ootacamund, India

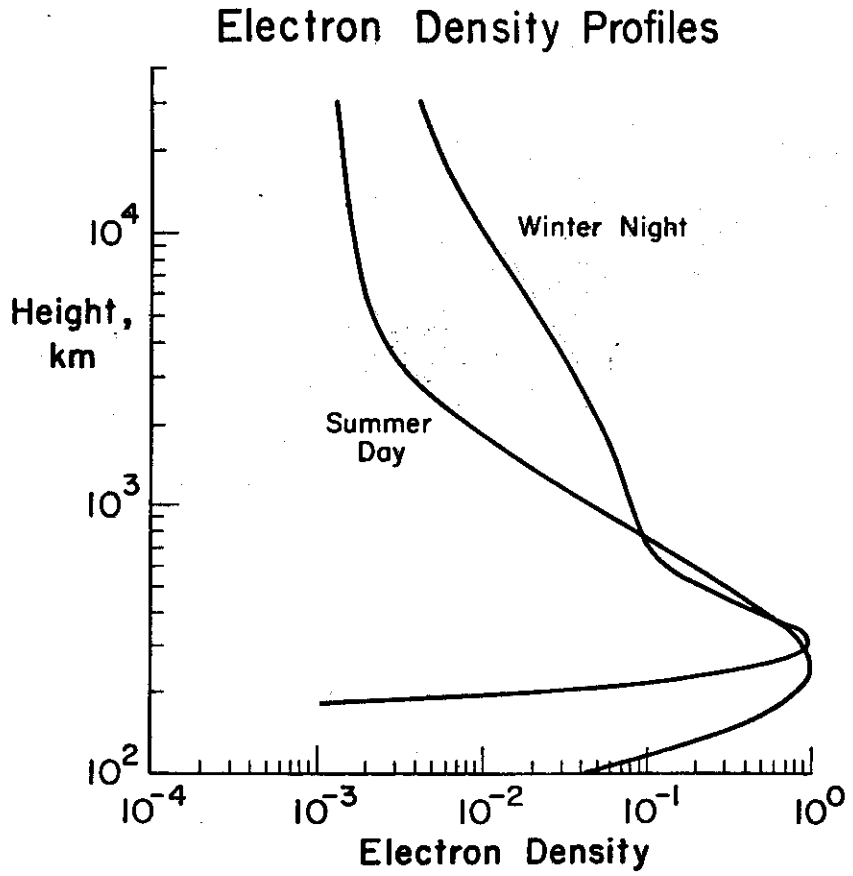

Fig. 5.9 Electron density profiles obtained from satellite beacon measurements, Boulder

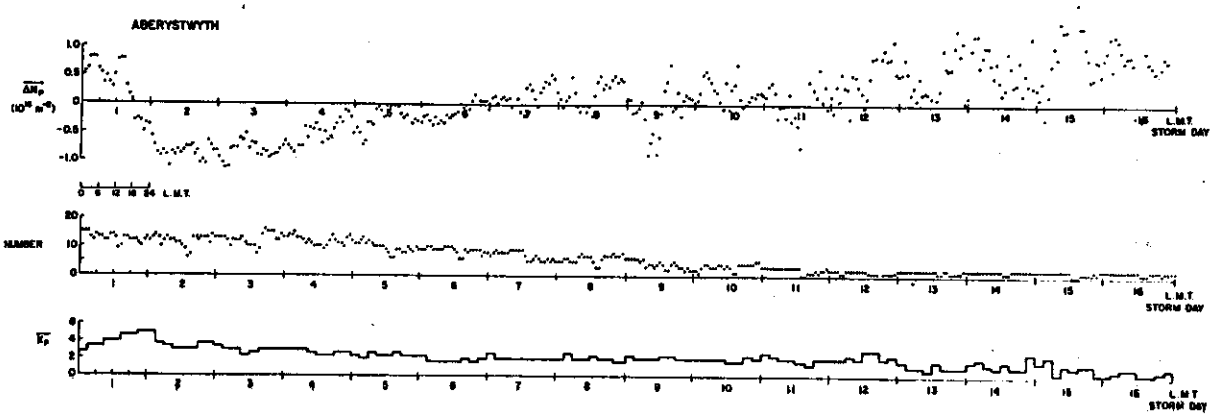

Fig. 5.10 Storm behavior of the plasmasphere contents

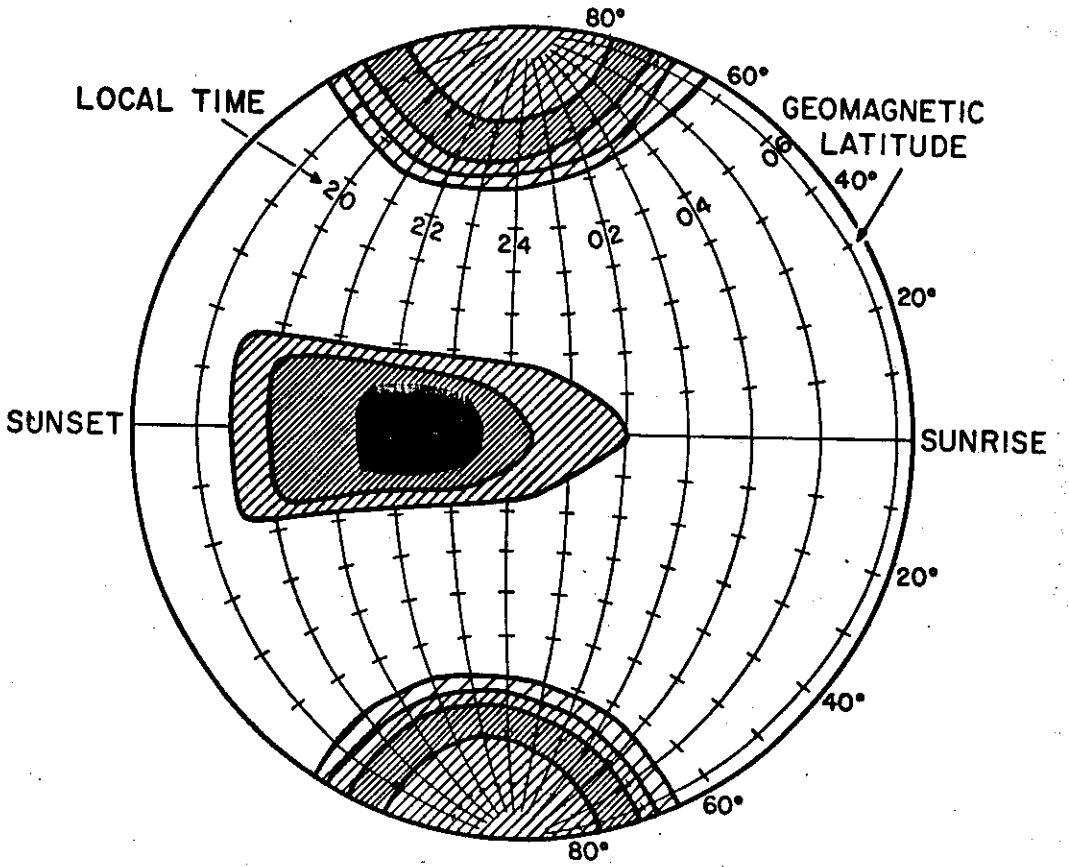

Fig. 5.11 Morphology of scintillation fading

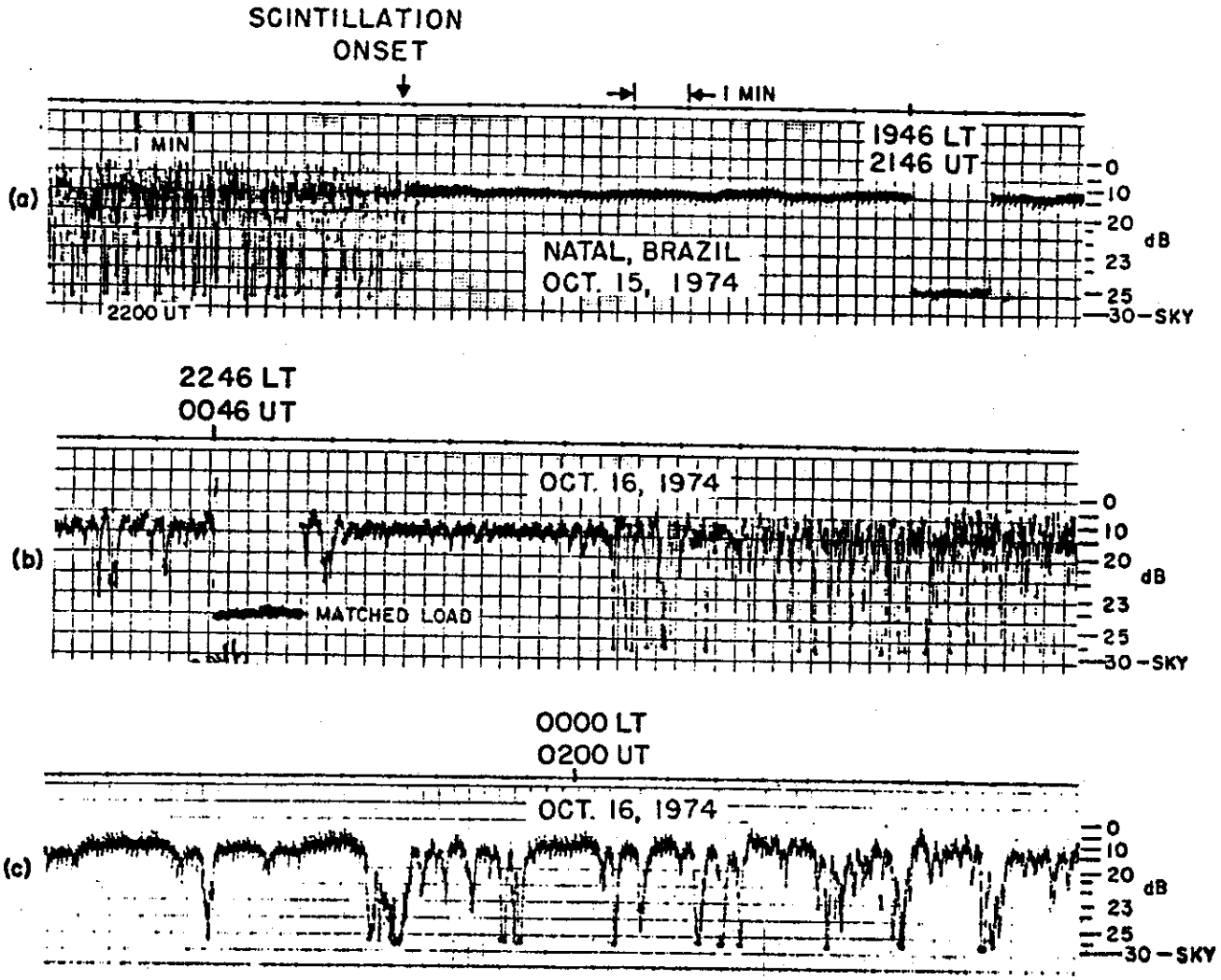

Fig. 5.12 Abrupt changes in scintillation

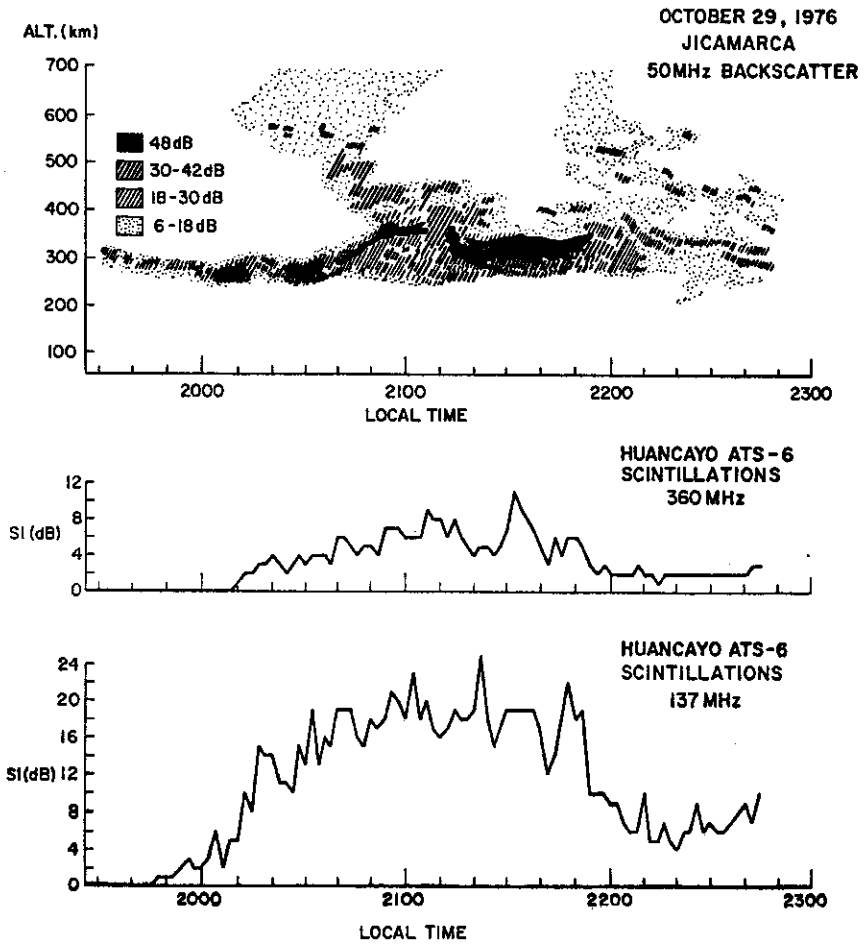

Fig. 5.13 Incoherent scatter plumes and satellite radio scintillation near the equator.

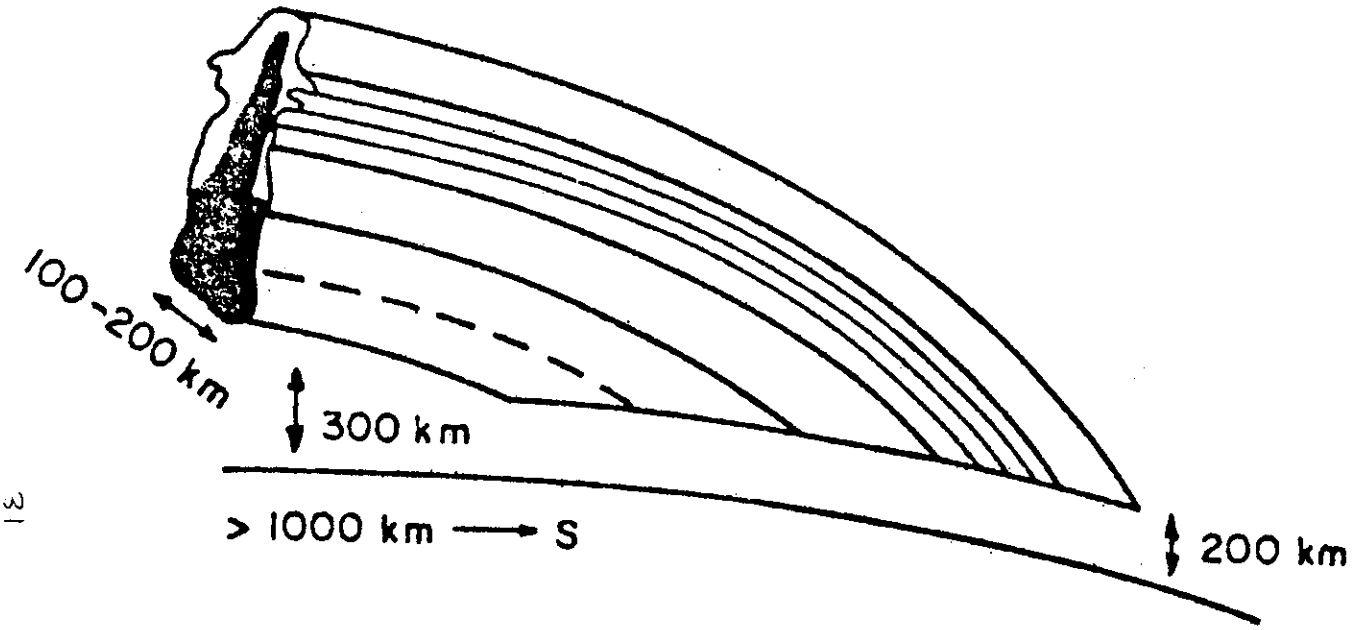

THREE DIMENSIONAL
PATCH MODEL

Fig. 5.14 Three-dimensional patch model of equatorial ionospheric irregularities

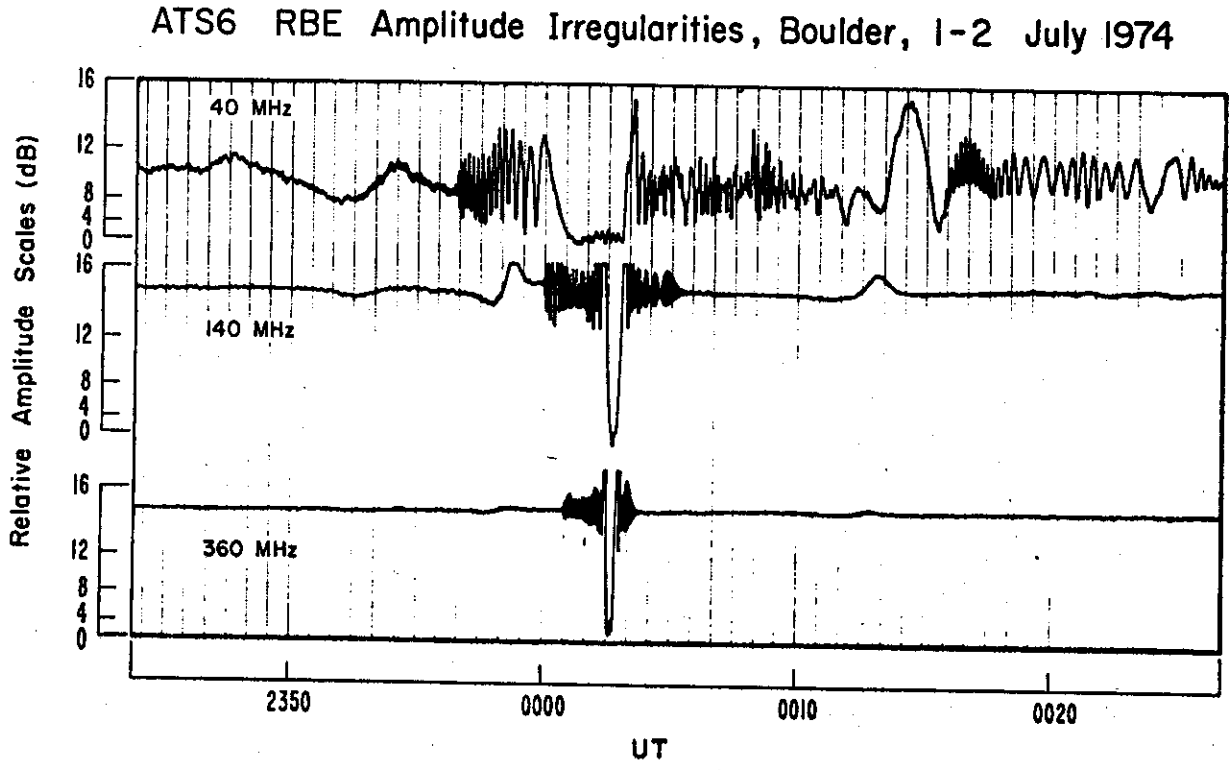

Fig. 5.15 Fading of ATS6-Boulder signals caused by an intense irregularity.

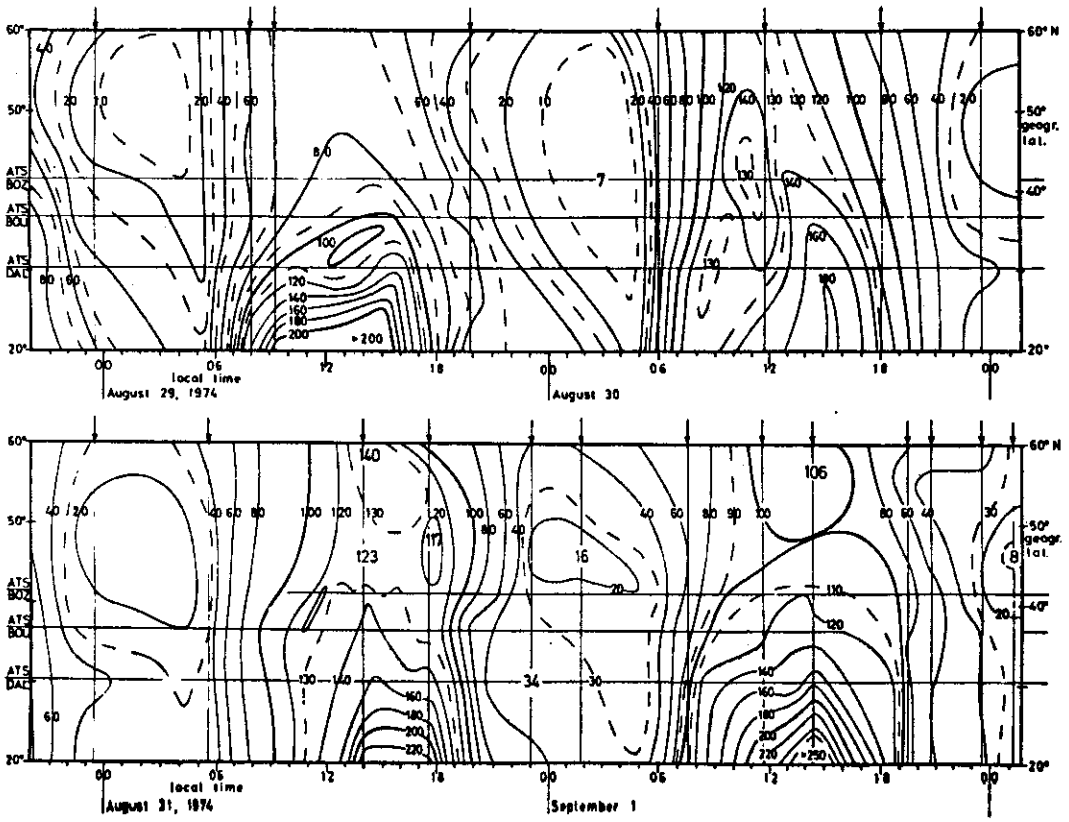

Fig. 5.16 Contour map of TEC in latitude versus time, in TEC units of 10^{15} m^{-2}.
Separation of solid lines $\approx$ 20 x 10^{15} m^{-2}.